Scenario-Oriented Multi-Cut Generalized Benders Decomposition-Based Distributed OPF for AC/DC Hybrid Grids

Li, Hai Xiao; Ergun, Hakan; Van Hertem, Dirk; Lekic, Aleksandra

DOI
10.1109/ISGTEUROPE62998.2024.10863082

Publication date
2024

Document Version
Final published version

Published in
IEEE PES Innovative Smart Grid Technologies Europe, ISGT EUROPE 2024

Scenario-Oriented Multi-Cut Generalized Benders Decomposition-Based Distributed OPF for AC/DC Hybrid Grids

Hai-Xiao Li[1,2], Hakan Ergun[3], Dirk Van Hertem[3], Aleksandra Lekić[1]
[1]*Faculty of Electrical Engineering, Mathematics & Computer Science, Delft University of Technology, Delft, The Netherlands*
[2]*School of Electrical and Electronic Engineering, Chongqing University of Technology, Chongqing, China*
[3]*Electa, Department of Electrical Engineering, KU Leuven, Leuven, Belgium, and also with Etch-EnergyVille, Genk*
{H.Li-16, A.Lekic}@tudelft.nl, {hakan.ergun, dirk.vanhertem}@kuleuven.be

2024 IEEE PES Innovative Smart Grid Technologies Europe (ISGT EUROPE) | 979-8-3503-9042-1/24/$31.00 ©2024 IEEE | DOI: 10.1109/ISGTEUROPE62998.2024.10863082

***Abstract*—In this paper, a distributed optimal power flow (OPF) for the AC/DC hybrid grid, composed of the AC grid, renewable energy system (RES), and voltage source converter (VSC)-based multi-terminal DC (MTDC) grid, is presented. Firstly, we apply a series of linear approximations/convex relaxations to construct a mixed-integer convex AC/DC OPF model. To address the uncertainties from RESs, we then illustrate scenario-oriented decision making for the constructed AC/DC OPF model. Additionally, we verify that considering all possible scenarios can be replaced by a small set of extreme scenarios if the OPF model is (mixed-integer) convex. Furthermore, we develop a scenario-oriented multi-cut generalized Benders decomposition to achieve more efficient distributed problem solving for the constructed AC/DC OPF model. Finally, numerical results are provided to validate the effectiveness of our constructed AC/DC OPF model and our developed distributed problem-solving approach.**

***Keywords*—*AC/DC hybrid grid*, *optimal power flow*, *extreme scenarios*, *generalized Benders decomposition*.**

I. Introduction

A. Background

The utilization of multi-terminal DC (MTDC) grids, comprising voltage-source converters (VSCs), has emerged as a promising solution for efficiently transmitting substantial power generated by renewable energy systems (RESs) to the remote AC grid. As a powerful tool, the optimal power flow (OPF) technique offers many advantages for the safe and economical operation of such AC/DC hybrid grids [1]. However, the application of OPF models still encounters numerous challenges. A prominent one of these challenges is that archival centralized optimization is unsuitable for hybrid grids involving multiple entities. Hence, it is unsurprising that many studies have focused on distributed optimization [2-5].

In terms of model accuracy, there is no doubt that nonconvex OPF models based on the well-known nonlinear power flow equations are the most preferred. However, nonconvex models cannot guarantee the rigorous convergence for some widely used distributed optimization algorithms [2-3]. In recent times, groundbreaking work has been laid in [4]. The augmented Lagrangian alternating direction inexact Newton (ALADIN) method is utilized for the generalized nonconvex AC OPF model. Subsequently, [5] extends the application of ALADIN to the nonconvex AC/DC OPF model. Although ALADIN excels in distributedly solving nonconvex optimization problems, its scalability is relatively limited as it cannot handle integer variables, which are inevitably introduced in the AC/DC OPF model to account for unit commitment and topology reconfiguration in the AC/DC grid [6].

This work was supported by CRESYM project Harmony (https://cresym.eu/harmony/).

Many studies have investigated various linear approximations and convex relaxations of the power flow equations in AC and DC grids [7-9]. With the help of these techniques, the (mixed-integer)convex AC/DC OPF model is formulated. In this case, popular distributed optimization algorithms, like the alternating direction method of multipliers (ADMM) (for convex programming) [2] or generalized Benders decomposition (GBD) (for mixed-integer convex programming) [3], can be adopted. Although feasible solutions are presented in the literature mentioned above, the model-building and problem-solving aspects of the distributed AC/DC OPF problem still need improvement in terms of scalability, handling uncertainties, and considering the influence of local control behavior of VSCs.

B. Main Contributions

Our work on the distributed AC/DC OPF for the hybrid grid is motivated by two key questions: i) *How to consider the influences of uncertainties from RESs and the droop control of VSCs*? ii) *How can we enhance the performance of the selected distributed optimization approach*? Our main contributions are listed below.

- This work constructs a specific mixed-integer convex AC/DC OPF model to formulate the steady-state behavior of the hybrid AC/DC grid. Besides, the impact of the VSC droop control on OPF decision making is explicitly formulated.
- This work converts the constructed AC/DC OPF model from the conventional deterministic formulation to the scenario-oriented formulation, addressing the uncertainties from RESs. Further, we mitigate the computational burden by considering the few extreme scenarios replacing massive possible scenarios, and demonstrate that this approach applies well to convex optimization problems.
- We select GBD to solve the scenario-oriented AC/DC OPF model (considering that integer variables are involved) and modify the cut-returning procedure in the traditional GBD by partitioning slave problems according to the system types (AC grid or RES) and extreme scenarios. Then, we utilize the multi-cut generation technique [10] to enable parallel computation among the AC grid and RESs while enhancing the convergence rate.

The paper begins with the AC/DC OPF mathematical formulation in Section II. Then, scenario-oriented decision making is introduced in Section III, and GBD-based distributed problem solving is presented in Section IV. Numerical studies are presented and discussed in Section V, followed by the conclusion drawn in Section VI.

II. Mixed-Integer Convex AC/DC OPF Model

A. Linear Constraints for the AC Grid

The nonlinear AC grid power flow on a branch (i, j) can be linearized by the successive linear approximation [9]:

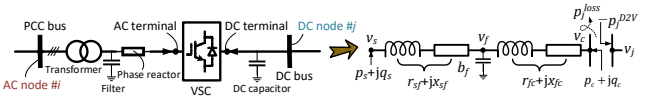

Fig. 1. Equivalent impedance model of the VSC station.

$$p_{ij} = g_{ij}u_i - g_{ij}^{P,k}\frac{u_i+u_j}{2} - b_{ij}^{P,k}\left(\theta_{ij}-\theta_{ij,k}\right) + g_{ij}^{P,k}\frac{v_{ij,L}^{s}}{2}, \quad (1a)$$

$$q_{ij} = b_{ij}^{Q,k}\frac{u_i+u_j}{2} - b_{ij}u_i - g_{ij}^{Q,k}\left(\theta_{ij}-\theta_{ij,k}\right) - b_{ij}^{Q,k}\frac{v_{ij,L}^{s}}{2}, \quad (1b)$$

$$\forall i \in \mathbb{m}^{AC}, \qquad \forall (i,j) \in \mathbb{l}^{AC}$$

where $\mathbb{m}^{AC}$ and $\mathbb{l}^{AC}$ are used to denote the node and branch sets for the AC grid. $g_{ij}^{P,k}, b_{ij}^{P,k}, g_{ij}^{Q,k}, b_{ij}^{Q,k}, \theta_{ij,k}, v_{ij,L}^{s}$ are the determined parameters associated with the initial power flow points. g_{ij}/b_{ij} is the conductance/susceptance. u_i, the square of the nodal voltage v_i, treated as an independent variable, enables the branch active/reactive power flow p_{ij}/q_{ij} with linear expression. More details can be found in [9].

According to (1), (2) representing nodal power injection on node i can be derived, such that:

$$p_i = \sum_{(i,j)} p_{ij} + u_i \sum_j G_{ij}, \quad (2a)$$

$$q_i = \sum_{(i,j)} q_{ij} - u_j \sum_j B_{ij}, \quad (2b)$$

$$p_i = p_i^G - p_i^D - p_i^{A2V},\ q_i = q_i^G - q_i^D - q_i^{A2V}, \quad (2c)$$

$$\forall i \in \mathbb{m}^{AC}, \qquad \forall (i,j) \in \mathbb{l}^{AC}$$

where G_{ij}/B_{ij} is the real/imaginary part of Y_{ij} in the admittance matrix. p_i^G/q_i^G (resp. p_i^D/q_i^D) represents the active/reactive power produced (resp. power consumed) by generators (resp. demands). p_i^{A2V}/q_i^{A2V} represents the active/reactive power transmitted from the AC grid to the VSC station. Nodal active power injection p_i (resp. reactive power injection q_i) is contributed by p_i^G, p_i^D, p_i^{A2V} (resp. q_i^G, q_i^D, q_i^{A2V}). If node i is not connected to the generator (resp. the VSC station), then $p_i^G = 0, q_i^G = 0$ (resp. $p_i^{A2V} = 0, q_i^{A2V} = 0$).

The remaining operational constraints are:

$$-\overline{s}_{ij} \le \cos\left(\frac{n\pi}{\mathcal{N}_n}\right)p_{ij} + \sin\left(\frac{n\pi}{\mathcal{N}_n}\right)q_{ij} \le \overline{s}_{ij}, \quad (3a)$$

$$-\overline{s}_i^G \le \cos\left(\frac{n\pi}{\mathcal{N}_n}\right)p_i^G + \sin\left(\frac{n\pi}{\mathcal{N}_n}\right)q_i^G \le \overline{s}_i^G, \quad (3b)$$

$$\underline{u}_i \le u_i \le \overline{u}_i, \quad (3c)$$

$$\forall i \in \mathbb{m}^{AC}, \qquad \forall (i,j) \in \mathbb{l}^{AC}, \qquad \forall n \in \{1,\cdots,\mathcal{N}_n\}$$

where we use $\underline{*}/\overline{*}$ to represent the lower/upper bound of variables. (3a) is the linearized constraint to approximate the nonlinear equation that $0 \le s_{ij}^2 = p_{ij}^2 + q_{ij}^2 \le \overline{s}_{ij}^2$. The apparent power s_{ij} following the branch is constrained by using an N-vertex polygon approximation and defining a polyhedral norm [11]. Similarly, (3b) is the approximated linearized constraint that is used to constrain the apparent power s_i^G produced by the generator. (3c) regulates the allowable range of the squared nodal voltage u_i.

B. Linear Constraints for the RES

RES l is simplified to a PQ node, which satisfies the constraint below:

$$-\overline{s}_l^R \le \cos\left(\frac{n\pi}{\mathcal{N}_n}\right)p_l^R + \sin\left(\frac{n\pi}{\mathcal{N}_n}\right)q_l^R \le \overline{s}_l^R, 0 \le p_l^R \le \overline{p}_l^R, \quad (4a)$$

$$p_l^R = p_l^{R2V}, q_l^R + q_l^{add} = q_l^{R2V}, \quad (4b)$$

$$\forall l \in \{1,\cdots,\mathcal{N}_l\}, \qquad \forall n \in \{1,\cdots,\mathcal{N}_n\}$$

where p_l^R, q_l^R, s_l^R represent the active, reactive, and apparent power produced by the RES. (4a) regulates that p_l^R, q_l^R should not exceed the RES-rated capacity $\overline{s}_l^R$. p_l^R should not exceed the available maximum power $\overline{p}_l^R$ that are affected by natural factors like solar radiance and wind speed. p_l^{R2V}/q_l^{R2V} represents the active/reactive power transmitted from the RES to the VSC station. In this study, the RES is considered to operate in the grid-connected mode, thus we have (4b), and q_l^{add} is the additional reactive power provided by var compensation devices (e.g., STATCOM) installed at the RES.

C. Convex Constraints for the MTDC Grid

The nonlinear DC grid power flow can be handled by SOC relaxation [7]:

$$p_i = \sum_{(i,j)} p_{ij},\ p_{ij} + p_{ji} = r_{ij}l_{ij}, \quad (5a)$$

$$u_i - u_j = r_{ij}\left(p_{ij} - p_{ji}\right),\ p_{ij}^2 \le l_{ij}u_i, \quad (5b)$$

$$p_i = -p_i^{M2V}, q_i = -q_i^{M2V}, \quad (5c)$$

$$\underline{u}_i \le u_i \le \overline{u}_i, \quad (5d)$$

$$\forall i \in \mathbb{m}^{MTDC}, \qquad \forall (i,j) \in \mathbb{l}^{MTDC}$$

where $\mathbb{m}^{MTDC}$ and $\mathbb{l}^{MTDC}$ are used to denote the node and branch sets for the MTDC grid. l_{ij} represents the squared branch current i_{ij}. (5a)-(5b) forms SOC relaxation of DC power flow by relaxing the inherent equation that $p_{ij} = i_{ij}v_i$. (5c) specify the nodal power injection. p_i^{M2V}/q_i^{M2V} denote the active/reactive power transmitted from the MTDC grid to the VSC station. (5d) regulates the allowable range of the squared nodal voltage u_i.

D. Mixed-Integer Convex Constraints for the VSC Station

The nonlinear AC power flow on the AC side of the VSC station (i.e. from the PCC bus to the AC terminal, as depicted in Fig. 1) can be handled by SOC relaxation[1] [8]:

$$p_i = c_{ii}G_{ii} + \sum_{(i,j)}\left(c_{ij}G_{ij} - s_{ij}B_{ij}\right), \quad (6a)$$

$$q_i = -c_{ii}B_{ii} - \sum_{(i,j)}\left(c_{ij}B_{ij} + s_{ij}G_{ij}\right), \quad (6b)$$

$$c_{ij} = c_{ji}, s_{ij} = -s_{ji}, c_{ij}^2 + s_{ij}^2 \le c_{ii}c_{jj}, \quad (6c)$$

$$c_{ii} = u_i,\ \underline{u}_i \le u_i \le \overline{u}_i, \quad (6d)$$

$$\forall i \in \mathbb{m}^{VSC}, \qquad \forall (i,j) \in \mathbb{l}^{VSC}$$

where $\mathbb{m}^{VSC}$ and $\mathbb{l}^{VSC}$ are used to denote the node and branch sets for the VSC staton AC side. In (6), c_{ii}, c_{ij}, s_{ij} are the introduced variables that have links with the squared nodal voltage u_i. Given that $u_i := e_i^2 + f_i^2$, then we have that $u_i = c_{ii} := e_i^2 + f_i^2, c_{ij} := e_ie_j + f_if_j, s_{ij} := e_if_j - e_jf_i$. SOC relaxation of AC power flow is formed by relaxing the instructive equation that $c_{ij}^2 + s_{ij}^2 = c_{ii}c_{jj}$. Besides, p_i, q_i for the VSC station can be specifically expressed as:

$$p_s = p_i^{A2V} \vee p_s = p_i^{R2V},\ p_f = 0,\ p_c = p_j^{M2V} - p_j^{loss}, \quad (7a)$$

$$q_s = q_i^{A2V} \vee q_s = q_i^{R2V},\ q_f = u_f b_f,\ q_c = q_j^{M2V}, \quad (7b)$$

$$\forall i \in \mathbb{m}^{AC}, \qquad \{s,f,c\} \in \mathbb{m}^{VSC}, \qquad \forall j \in \mathbb{m}^{MTDC}$$

where we use $\vee$ to represent the concept either. p_j^{loss} is the power loss inside the VSC station.

To better explain how to formulate voltage and power couplings between VSC AC and DC terminals, we first give the original nonlinear formulation, such that:

$$v_c = \delta v_j, 0 \le \delta \le \overline{\delta}, p_c + p_j + p_j^{loss} = 0, \quad (8a)$$

$$p_j^{loss} = a_{1c}i_c^2 + a_{2c}i_c + a_{3c}, \quad (8b)$$

$$i_c = \sqrt{(p_c^2 + q_c^2)/v_c^2}, 0 \le i_c \le \overline{i}_c, \quad (8c)$$

$$c \in \mathbb{m}^{VSC}, \qquad \forall j \in \mathbb{m}^{MTDC}$$

where (8a) indicates the voltage and power couplings between the AC and DC terminals. δ denotes the amplitude modulation factor of PWM. (8b) and (8c) indicate that the

[1]SOC relaxation [8] can also be an option to handle (1). However, commonly used off-the-shelf optimizers possibly fail to provide the high-fidelity extraction of duals for SOCP problem (https://github.com/jump-dev/Gurobi.jl/issues/415), which would affects the GBD iteration procedure.

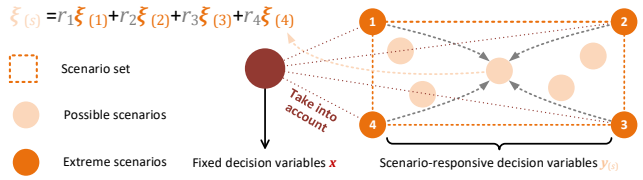

Fig . 2. Illustration regarding scenario-oriented decision making.

power loss inside the VSC station is a quadratic function with respect to i_c, which is the magnitude of current fflowing through the VSC station. $a_{1c}/a_{2c}/a_{3c}$ is the quadratic/linear/constant loss coefficient.

We take three key steps to handle (8): **(i)** u_c takes the place of v_c to express the nodal voltage to be compatible with the SOC relaxed power flow constraint (6). **(ii)** The quadratic term i_c^2 is handled by bivariate quadratic relaxation [12]. **(iii)** The nonlinear equation $i_c = \sqrt{(p_c^2 + q_c^2)/v_c^2}$ is handled by SOC relaxation. Consequently, we have the following mixed-integer convex constraints:

$$u_c \le \left(\overline{\delta}\right)^2 u_j,\ p_c + p_j + p_j^{loss} = 0, \tag{9a}$$

$$p_j^{loss} = a_{1c} l_c + a_{2c} i_c + a_{3c}, \tag{9b}$$

$$l_c \ge \textstyle\sum_k i_{c,q}^2,\ l_c \le \sum_q \{\overline{i}_{c,q} i_{c,q} + \underline{i}_{c,q} i_{c,q} - \overline{i}_{c,q}\underline{i}_{c,q} b_q\}, \tag{9c}$$

$$\textstyle\sum_q b_q = 1, \sum_q i_{c,q} = i_c,\ \underline{i}_{c,q} b_q \le i_{c,q} \le \overline{i}_{c,q} b_q, \tag{9d}$$

$$\underline{i}_{c,q} = \frac{\overline{i}_c(q-1)}{\mathcal{N}_q}, \overline{i}_{c,q} = \frac{\overline{i}_c q}{\mathcal{N}_q}, \tag{9e}$$

$$c \in \mathbb{m}^{VSC}, \quad \forall j \in \mathbb{m}^{MTDC}, \quad \forall q \in \{1, \cdots, \mathcal{N}_q\}$$

where (9a)-(9b) correspond to step **(i)**, (9c)-(9e) correspond to step **(ii)**, and (9f) corresponds to step **(iii)**. A total of $\mathcal{N}_q$ subranges are divided. $i_{c,q}$ denotes the variable within the qth subrange $[\underline{i}_{c,q}, \overline{i}_{c,q}]$, and the binary variable $b_q \in \{0,1\}$ is used to denote the status of each subrange, whether it is enabled (binary-1) or disabled (binary-0). (9c)-(9e) provide a tight convex envelope to approximate that $l_c := i_c^2$.

Furthermore, we consider the impact of VSC droop control on OPF decision making. Particularly, V^2-P droop control is considered here [13], and the function can be expressed as:

$$p_j = k_j^{drp}\left(u_j - u_j^{ref}\right) + p_j^{ref}, \tag{10a}$$

$$\underline{k}_j^{drp} \le k_j^{drp} \le 0,\ \underline{u}_j \le u_j^{ref} \le \overline{u}_j, \tag{10b}$$

$$\forall j \in \mathbb{m}^{MTDC}$$

where u_j^{ref}, p_j^{ref} denote voltage and power references in the droop control function. k_j^{drp} is the droop slope.

To improve droop control performance, the droop control parameters $u_j^{ref}, p_j^{ref}, k_j^{drp}$ are regarded as optimization variables. In this way, bilinear terms $k_j^{drp} u_j$ and $k_j^{drp} u_j^{ref}$ are involved. We handle them using McCormick evenlope, e.g., $U_j := k_j^{drp} u_j$ can be approximated as:

$$U_j \ge \underline{k}_j^{drp} \cdot u_j + \underline{u}_j \cdot k_j^{drp} - \underline{k}_j^{drp} \cdot \underline{u}_j, \tag{11a}$$

$$U_j \ge 0 \cdot u_j + \overline{u}_j \cdot k_j^{drp} - 0 \cdot \overline{u}_j, \tag{11b}$$

$$U_j \le \underline{k}_j^{drp} \cdot u_j + \overline{u}_j \cdot k_j^{drp} - \underline{k}_j^{drp} \cdot \overline{u}_j, \tag{11c}$$

$$U_j \le 0 \cdot u_j + \underline{u}_j \cdot k_j^{drp} - 0 \cdot \underline{u}_j. \tag{11d}$$

Besides, $U_j^{ref} := k_j^{drp} u_j^{ref}$ can be approximated with a set of constraints that are similar to (11). Eventually, (10a) is rewritten as a linear equation, such that:

$$p_j - p_j^{ref} = U_j - U_j^{ref}. \tag{12}$$

E. Quadratic Optimization Objective for the AC/VSC-MTDC Hybrid Power System

Regarding the optimization objective, we consider minimizing the generation costs and the total power losses (including AC line losses, DC line losses, and converter losses), such that:

$$min \left\{ \underbrace{\textstyle\sum_i \{c_{1i}(p_i^G)^2 + c_{2i} p_i^G + c_{3i}\}}_{generation\ costs} + \underbrace{\textstyle\sum_i \{p_i^G - p_i^D\} + \sum_l p_l^R}_{total\ power\ losses} \right\},$$
$$\forall i \in \mathbb{m}^{AC},\ \forall l \in \{1, \cdots, \mathcal{N}_l\} \tag{13}$$

where the generation cost is a quadratic function with respect to p_i^G . $c_{1i}/c_{2i}/c_{3i}$ is the quadratic/linear/constant cost coefficient. Total power losses can be calculated by subtracting load demands from power generation.

III. Scenario-Oriented Decision Making

The OPF problem formulated in (1)-(12) is deterministic (abbrev. D-OPF). The effectiveness of D-OPF is affected by: **(i)** Uncertain $\overline{p}_l^R$ related to the RES. **(ii)** Droop control influences related to VSC. Due to these reasons, D-OPF cannot fully reflect the operational status of the AC/DC hybrid power grid. In this regard, the concept of possible scenarios is introduced, and a scenario-oriented OPF (abbrev. S-OPF) model is formulated as below:

$$\begin{gathered} min\ \textstyle\sum_s F_{(s)}(\boldsymbol{\xi}_{(s)}, \boldsymbol{x}, \boldsymbol{y}_{(s)}) \\ s.t.\ \boldsymbol{G}_{(s)}\left(\boldsymbol{\xi}_{(s)}, \boldsymbol{x}, \boldsymbol{y}_{(s)}\right) \le 0, \boldsymbol{H}_{(s)}\left(\boldsymbol{\xi}_{(s)}, \boldsymbol{x}, \boldsymbol{y}_{(s)}\right) = 0' \\ \forall s \in \boldsymbol{S} \end{gathered} \tag{14}$$

where we use $*_{(s)}$ to represent the variable in the possible scenario s. $\boldsymbol{S}$ denote the set that covers all possible scenario s. $\boldsymbol{\xi}_{(s)}$ refers to $\overline{p}_l^R$ which is regarded as the uncertain variable. $\boldsymbol{x}, \boldsymbol{y}_{(s)}$ are decision variable vectors. $\boldsymbol{x}$ refers to the droop control parameters $U_j^{ref}, u_j^{ref}, p_j^{ref}, k_j^{drp}$ and they keep fixed among different scenario s. $\boldsymbol{y}_{(s)}$ are the remaining decision variables that respond to possible scenario changes. We can see that $\boldsymbol{x}$ is crucial and needs to be decided before $\boldsymbol{y}_{(s)}$ since it cannot be adjusted when encountering different possible scenarios. As indicated in (14), to guarantee the existence of feasible $\boldsymbol{y}_{(s)}$, an intuitive way is to list the constraints rrelatedto all possible scenarios, but it is evidently mass computation. Fortunately, if the S-OPF problem is convex, considering extreme scenarios e is sufficient, which will significantly reduce the computation cost, and (14) can be reduced to:

$$\begin{gathered} min\ \textstyle\sum_e F_{(e)}(\boldsymbol{\xi}_{(e)}, \boldsymbol{x}, \boldsymbol{y}_{(e)}) \\ s.t.\ \boldsymbol{G}_{(e)}\left(\boldsymbol{\xi}_{(e)}, \boldsymbol{x}, \boldsymbol{y}_{(e)}\right) \le 0, \boldsymbol{H}_{(e)}\left(\boldsymbol{\xi}_{(e)}, \boldsymbol{x}, \boldsymbol{y}_{(e)}\right) = 0' \\ \forall e \in \boldsymbol{\mathcal{E}} \subseteq \boldsymbol{S} \end{gathered} \tag{15}$$

where we use $*_{(e)}$ to represent the variable in the extreme scenario e. $\boldsymbol{\mathcal{E}}$ denote the set that covers all possible scenario e. More specifically, assuming a fluctuation range of $\boldsymbol{\xi}_{(s)}$ is $[\underline{\boldsymbol{\xi}}, \overline{\boldsymbol{\xi}}]$, the extreme scenario refer that $\boldsymbol{\xi}_{(e)} := \underline{\boldsymbol{\xi}} \vee \overline{\boldsymbol{\xi}}$.

We provide the illustration in Fig. 2 and give the proof [14]-[15]. Given that $\sum_e r_e = 1, r_e \ge 0$, we can know that arbitrary $\boldsymbol{\xi}_{(s)}$ can be expressed as $\boldsymbol{\xi}_{(s)} = \sum_e r_e \boldsymbol{\xi}_{(e)}$. Review (1)-(12), constraints in (15) can be further expressed as :

$$\boldsymbol{H}_{(e)}\left(\boldsymbol{\xi}_{(e)}, \boldsymbol{x}, \boldsymbol{y}_{(e)}\right) := \boldsymbol{A}_H \boldsymbol{\xi}_{(e)} + \boldsymbol{B}_H \boldsymbol{x} + \boldsymbol{C}_H \boldsymbol{y}_{(e)} = 0, \tag{16a}$$

$$\boldsymbol{G}_{a(e)}\left(\boldsymbol{\xi}_{(e)}, \boldsymbol{x}, \boldsymbol{y}_{(e)}\right) := \boldsymbol{A}_G \xi_{(e)} + \boldsymbol{B}_G \boldsymbol{x} + \boldsymbol{C}_G \boldsymbol{y}_{(e)} \le 0, \tag{16b}$$

$$\boldsymbol{G}_{b(e)}\left(\boldsymbol{\xi}_{(e)}, \boldsymbol{x}, \boldsymbol{y}_{(e)}\right) := \left\| \boldsymbol{D} \circ \left[\boldsymbol{\xi}_{(e)}, \boldsymbol{x}, \boldsymbol{y}_{(e)}\right]^{\mathrm{T}} \right\|_2 - \boldsymbol{E}\left[\boldsymbol{\xi}_{(e)}, \boldsymbol{x}, \boldsymbol{y}_{(e)}\right]^{\mathrm{T}} \le 0, \tag{16c}$$

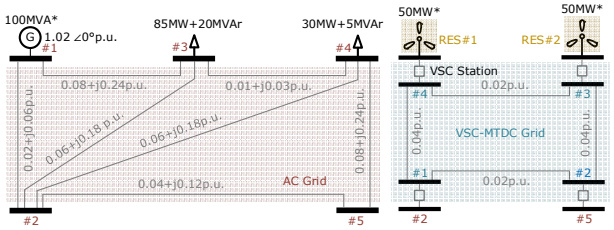

Fig. 3. Test system of the AC/DC hybrid grid.

where $\boldsymbol{A}_{H/G}, \boldsymbol{B}_{H/G}, \boldsymbol{C}_{H/G}, \boldsymbol{D}, \boldsymbol{E}$ are the coefficient matrix. (16a) and (16b) corresponds to linear equality constraints and inequality constraints, respectively. (16c) corresponds to SOC relaxed convex constraints.

Further, we can deduce the following relationship based on the linear rules:

$$0 = \sum_e \{r_e \boldsymbol{H}_{(e)}(\boldsymbol{\xi}_{(e)}, \boldsymbol{x}, \boldsymbol{y}_{(e)})\} = \boldsymbol{H}_{(e)}\left(\sum_e r_e \boldsymbol{\xi}_{(e)}, \boldsymbol{x}, \sum_e r_e \boldsymbol{y}_{(e)}\right) \Rightarrow \boldsymbol{H}_{(s)}(\boldsymbol{\xi}_{(s)}, \boldsymbol{x}, \boldsymbol{y}_{(s)}) = 0, \quad (17a)$$

$$0 \geq \sum_e \{r_e \boldsymbol{G}_{a(e)}(\boldsymbol{\xi}_{(e)}, \boldsymbol{x}, \boldsymbol{y}_{(e)})\} = \boldsymbol{G}_{a(e)}\left(\sum_e r_e \boldsymbol{\xi}_{(e)}, \boldsymbol{x}, \sum_e r_e \boldsymbol{y}_{(e)}\right) \Rightarrow \boldsymbol{G}_{a(s)}(\boldsymbol{\xi}_{(s)}, \boldsymbol{x}, \boldsymbol{y}_{(s)}) \leq 0 \quad (17b)$$

here (17) indicates that if linear constraints in all extreme scenarios e hold, then they, in all possible scenarios s hold.

Besides, according to Jensen's inequality, we have that:

$$\boldsymbol{G}_{b(e)}\left(\sum_e r_e \boldsymbol{\xi}_{(e)}, \boldsymbol{x}, \sum_e r_e \boldsymbol{y}_{(e)}\right) \leq \sum_e r_e\, \boldsymbol{G}_{b(e)}(\boldsymbol{\xi}_{(e)}, \boldsymbol{x}, \boldsymbol{y}_{(e)}) \leq 0 \Rightarrow \boldsymbol{G}_{b(s)}(\boldsymbol{\xi}_{(s)}, \boldsymbol{x}, \boldsymbol{y}_{(s)}) \leq 0 \quad (18)$$

here (18) indicates that if SOC constraints in all extreme scenarios e hold, then they, in all possible scenarios s hold.

IV. GBD-Based Distributed Problem Solving

We use GBD to solve (15) in a distributed manner. (15) can be reformulated as the combination of one master problem (MP) and several slave problems (SPs), such that:

$$min\ \sum_e F_{(e)}^{MP}\left(\boldsymbol{x}, \boldsymbol{w}_{(e)}^{MP}, \boldsymbol{z}_{(e)}^{MP}\right) + \sum_k \sum_e F_{k(e)}^{SP}\left(\boldsymbol{\xi}_{k(e)}, \boldsymbol{w}_{k(e)}^{SP}, \boldsymbol{z}_{k(e)}^{SP}\right)$$

$$s.t. \begin{cases} \underbrace{\boldsymbol{G}_{(e)}^{MP}\left(\boldsymbol{x}, \boldsymbol{w}_{(e)}^{MP}\right) \leq 0, \boldsymbol{H}_{(e)}^{MP}\left(\boldsymbol{x}, \boldsymbol{w}_{(e)}^{MP}\right) = 0}_{independent\ constaints\ in\ MP} \\ \underbrace{\boldsymbol{G}_{k(e)}^{SP}\left(\boldsymbol{\xi}_{k(e)}, \boldsymbol{w}_{k(e)}^{SP}\right) \leq 0, \boldsymbol{H}_{k(e)}^{SP}\left(\boldsymbol{\xi}_{k(e)}, \boldsymbol{w}_{k(e)}^{SP}\right) = 0}_{independent\ constraints\ in\ SP\ k} \\ \underbrace{\boldsymbol{H}_{k(e)}^{CP}\left(\boldsymbol{z}_{(e)}^{MP}, \boldsymbol{z}_{k(e)}^{SP}\right) = 0}_{coupling\ constraints\ between\ MP\ and\ SP\ k} \end{cases}, \quad (19)$$

$$\forall e \in \mathcal{E} \subseteq \mathcal{S}, \qquad \forall k \in \{1, \cdots, \mathcal{N}_k\}$$

where we use $*^{MP}$ to represent the objective, constraints, variables in MP and $*_k^{SP}$ to represent objectives, constraints, and variables in the SP k. MP is associated with the VSC-MTDC and SPs are associated with the AC systems (refers to the AC grid or RESs). x (refers to $U_j^{ref}, u_j^{ref}, p_j^{ref}, k_j^{drp}$) only appear in MP and $\xi_{(e)}$ (refers to $\overline{p}_{l,(e)}^{R}$) only appear in SPs. $\boldsymbol{y}_{(e)}$ splits into the independent $\boldsymbol{w}_{(e)}$ and coupled $\boldsymbol{z}_{(e)}$.

GBD begins with solving SPs. Notice that: **(i)** *There are no coupling constraints between arbitrary SP i and SP j, as the interconnection of any two AC systems is only via VSC-MTDC.* **(ii)** *There are no coupling constraints between arbitrary extreme scenario a and extreme scenario b, as SPs do not contain the fixed decision variables* $\boldsymbol{x}$. In this case, solving $min\ \sum_k \sum_e F_{k(e)}^{SP}(\boldsymbol{\xi}_{k(e)}, \boldsymbol{w}_{k(e)}^{SP}, \boldsymbol{z}_{k(e)}^{SP})$ equivalent to solving $\sum_k \sum_e min\ F_{k(e)}^{SP}(\boldsymbol{\xi}_{k(e)}, \boldsymbol{w}_{k(e)}^{SP}, \boldsymbol{z}_{k(e)}^{SP})$. Each original SP k in the extreme scenario e can be solved in parallel:

$$Orignal\ SP \mapsto min\ F_{k(e)}^{SP}(\boldsymbol{\xi}_{k(e)}, \boldsymbol{w}_{k(e)}^{SP}, \boldsymbol{z}_{k(e)}^{SP})$$
$$s.t.\ \boldsymbol{G}_{k(e)}^{SP}(\boldsymbol{\xi}_{k(e)}, \boldsymbol{w}_{k(e)}^{SP}) \leq 0, \boldsymbol{H}_{k(e)}^{SP}(\boldsymbol{\xi}_{k(e)}, \boldsymbol{w}_{k(e)}^{SP}) = 0$$

$$\boldsymbol{H}_{k(e)}^{CP}\left(\hat{\boldsymbol{z}}_{(e)}^{MP[v]}, \boldsymbol{z}_{k(e)}^{SP}\right) = 0 \mid \boldsymbol{\lambda}_{k(e)}, \quad (20)$$

where we use $\hat{*}^{[v]}$ to represent the determined variable value at the vth iteration in the GBD procedure. $\boldsymbol{\lambda}_{k(e)}$ is the dual multipliers corresponding to constraints $\boldsymbol{H}_{k(e)}^{CP} = 0$. The upper bound (ub) of (19) is provided by (20). If (20) is infeasible, a relaxed SP is formed and will be solved:

$$Relaxed\ SP \mapsto min\ \left\|\boldsymbol{\varepsilon}_{k(e)}\right\|_1 + \left\|\boldsymbol{\sigma}_{k(e)}\right\|_1$$
$$s.t.\ \boldsymbol{G}_{k(e)}^{SP}(\boldsymbol{\xi}_{k(e)}, \boldsymbol{w}_{k(e)}^{SP}) \leq 0, \boldsymbol{H}_{k(e)}^{SP}(\boldsymbol{\xi}_{k(e)}, \boldsymbol{w}_{k(e)}^{SP}) = 0$$
$$\boldsymbol{H}_{k(e)}^{CP}\left(\hat{\boldsymbol{z}}_{(e)}^{MP[v]}, \boldsymbol{z}_{k(e)}^{SP}\right) - \boldsymbol{\varepsilon}_{k(e)} \leq 0 \mid \boldsymbol{\mu}_{k(e)}^{\varepsilon}$$
$$-\boldsymbol{H}_{k(e)}^{CP}\left(\hat{\boldsymbol{z}}_{(e)}^{MP[v]}, \boldsymbol{z}_{k(e)}^{SP}\right) - \boldsymbol{\sigma}_{k(e)} \leq 0 \mid \boldsymbol{\mu}_{k(e)}^{\sigma} \quad (21)$$
$$\boldsymbol{\varepsilon}_{k(e)} \geqslant 0, \boldsymbol{\sigma}_{k(e)} \geqslant 0,$$

where $\boldsymbol{\varepsilon}_{k(e)}, \boldsymbol{\sigma}_{k(e)}$ are vectors composed of small positive numbers and utilized to relax $\boldsymbol{H}_{k(e)}^{CP} = 0$. $\boldsymbol{\mu}_{k(e)}^{\varepsilon}, \boldsymbol{\mu}_{k(e)}^{\sigma}$ are the dual multipliers of constraints $\boldsymbol{H}_{k(e)}^{CP} - \boldsymbol{\varepsilon}_{k(e)} \leq 0$, $-\boldsymbol{H}_{k(e)}^{CP} - \boldsymbol{\sigma}_{k(e)} \leq 0$. Conventionally, if one SP is infeasible, all SPs will be reformulated, i.e., uni-cut GBD (standard GBD version). This approach implies that solving SPs are not mutually independent. Considering this issue, the multi-cut generation technique is employed [10], and multi-cut GBD is formed. In this way, each SP will independently return a linear Benders cut to MP, such that:

$$\eta_{k(e)} \geq \hat{\mathcal{L}}_{k(e)}^{[v]} + \left(\nabla_{\boldsymbol{w}_{(e)}^{MP}} \mathcal{L}_{k(e)}\right)^{\mathsf{T}} \left(\boldsymbol{w}_{(e)}^{MP} - \hat{\boldsymbol{w}}_{(e)}^{MP[v]}\right) + \left(\nabla_{\boldsymbol{z}_{(e)}^{MP}} \mathcal{L}_{k(e)}\right)^{\mathsf{T}} \left(\boldsymbol{z}_{(e)}^{MP} - \hat{\boldsymbol{z}}_{(e)}^{MP[v]}\right), \quad (22a)$$

$$0 \geq \hat{\mathcal{H}}_{k(e)}^{[v]} + \left(\nabla_{\boldsymbol{z}_{(e)}^{MP}} \mathcal{H}_{k(e)}\right)^{\mathsf{T}} \left(\boldsymbol{z}_{(e)}^{MP} - \hat{\boldsymbol{z}}_{(e)}^{MP[v]}\right), \quad (22b)$$

$$\mathcal{L}_{k(e)} \coloneqq F_{(e)}^{MP} + F_{k(e)}^{SP} + \boldsymbol{\lambda}_{k(e)}^{\mathsf{T}} \boldsymbol{H}_{k(e)}^{CP}, \quad (22c)$$

$$\mathcal{H}_{k(e)} \coloneqq \boldsymbol{\mu}_{k(e)}^{\varepsilon\mathsf{T}} \boldsymbol{H}_{k(e)}^{CP} - \boldsymbol{\mu}_{k(e)}^{\sigma\mathsf{T}} \boldsymbol{H}_{k(e)}^{CP}, \quad (22d)$$

where (22a) is called the optimality cut, generated from (20) and (22b) is called the feasibility cut, generated from (21).

Consequently, MP is formulated as below and provides the lower bound (lb):

$$MP \mapsto \min \sum_k \sum_e \eta_{k(e)}, s.t.\ (22a), (22b), \quad (23)$$

Distributed problem solving for (15) is achieved by alternatively solving (20)(or (21)) and (23), until $|lb - ub|/|lb| \leq thr.$. It can be summarized that the division of SPs considers extreme scenario split and the cut generation is multiple at each iteration. *Hence, we name this approach as scenario-oriented multi-cut GBD (S-M-GBD).*

V. Numerical Experiments

We use the test system shown in Fig. 3 containing one 5-node AC grid, one 4-node VSC-MTDC grid, and two RESs. The base power and voltage of the test system are assumed to be 100MVA and 345kV, respectively. OPF problem is computed in per unit value. Key variable bounds are set as $[\underline{u}_i, \overline{u}_i] = [0.95, 1.05]\text{p.u.}, \forall i \in \mathbb{m}^{AC} \cup \mathbb{m}^{VSC} \cup \mathbb{m}^{MTDC}$. $\overline{s}_i^G = 1\text{p.u}$, $\overline{s}_{ij} = 1\text{p.u}$, $\forall i \in \mathbb{m}^{AC}$, $\forall (i,j) \in \mathbb{l}^{AC}$. $\overline{i}_c = 1\text{p.u.}$, $c \in \mathbb{m}^{VSC}$. $\underline{k}_j^{drp} = -1$, $\forall j \in \mathbb{m}^{MTDC}$. $\overline{\delta} = 1$. For fair performance comparison among GBD, M-GBD, and S-M-GBD, we initialize coupled voltage and power in these approaches to be consistent, as 1 and 0. $thr.$ and the maximum iteration number are set to 1e-3 and 50, respectively. The case study is coded on `MATLAB` platform. `YALMIP` toolbox is utilized to provide the mathematic programming modeling environment. `CPLEX` solver is invoked for solving the involved (mixed-integer)convex pro-

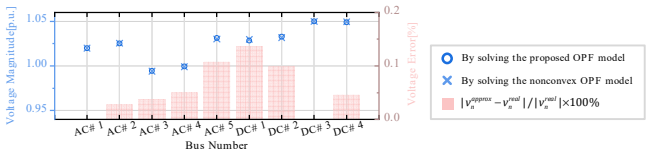

Fig. 4. Comparison of the calculated system-wide voltage profiles (solved via centralized optimization).

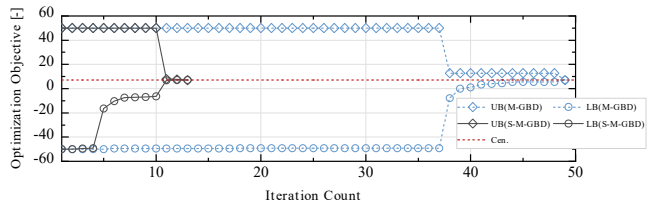

Fig. 5. Iteration process of M-GBD and S-M-GBD. M-GBD does not consider extreme scenario split when forming SPs.

TABLE I. OPTIMIZATION OBJECTIVE IN POSSIBLE SCENARIOS

Conventional decision making		Scenario-oriented decision making	
Expected/Worst	Feasible num.	Expected/Worst	Feasible num.
1.4115/1.5370	7	1.5082/1.8423	50

✧ The expected objective value is calculated based on $(\overline{p}_1^R, \overline{p}_2^R) = (0.5,0.5)\text{p. u.}$. $U_j^{ref}, u_j^{ref}, p_j^{ref}, k_j^{drp}$ are kept fixed and brought into the OPF models with different scenarios to examine whether feasible solution exists.

gramming problems.

We first evaluate the accuracy of the power flow calculation in our constructed AC/DC OPF model. The benchmark results are obtained by using `IPOPT` to solve the original nonconvex AC/DC OPF model with the determined $p_i^G, q_i^G, p_l^R, q_l^R, q_l^{add}$ that are obtained from solving the constructed mixed-integer convex AC/DC OPF model. The initial point involved in (1) starts with a flat power flow status and then switches to an updated power flow status (power injection at AC nodes #2 and #5 are changed to the optimized value from zero). The comparison of the system-wide voltage profiles is shown in Fig. 4. Although our constructed AC/DC OPF model employs a series of linear approximation/convex relaxations to handle the nonlinearity in power flow, it still exhibits a decent performance in power flow calculation. The maximum relative error of nodal voltage is less than 0.2%.

We subsequently illustrate the convergence rate of our proposed S-M-GBD. Four extreme scenarios are considered in our constructed AC/DC OPF model. They are assumed to be $(\overline{p}_1^R, \overline{p}_2^R) \in \{(0.5,0.5), (0.5,0.3), (0.4,0.5), (0.4,0.3)\}\text{p. u.}$. We compare the iteration numbers required for convergence among GBD, M-GBD, and S-M-GBD. Given the same initial iteration conditions, GBD fails to converge within 50 iterations. As shown in Fig. 5, M-GBD and S-M-GBD converge successfully and approach the centralized optimization result (as the benchmark). Compared with M-GBD, S-M-GBD consumed fewer iterations. This is because S-M-GBD forms SPs considering extreme scenario split, thus returning more Benders cuts to MP per iteration and thus enhancing the convergence rate.

We finally validate the robustness of the scenario-oriented decision making. Conventional decision making is implemented with just 1 deterministic scenario that $(\overline{p}_1^R, \overline{p}_2^R) = (0.5,0.5)\text{p. u.}$. In contrast, our proposed scenario-oriented decision making is implemented taking 4 extreme scenarios into account, which are consistent with the above-mentioned. We randomly generate 50 possible scenarios where $\overline{p}_1^R \in [0.4, 0.5]\text{p. u.}, \overline{p}_2^R \in [0.3, 0.5]\text{p. u.}$ to compare the two kinds of decision making. As shown in Table I, despite our proposed scenario-oriented decision making having a more conservative objective value, the optimized droop control parameters in S-OPF model can hedge the uncertainties caused by RESs in all possible scenarios, but the conventional D-OPF cannot achieve the equivalent performance.

VI. CONCLUSION

This work presents a distributed OPF model for the AC/DC grid depending upon linear approximation and convex relaxation on AC/DC power flow and GBD. The results show that the constructed mixed-integer convex AC/DC OPF model provides satisfactory accuracy in the system-wide power flow calculation. The proposed scenario-oriented decision making ensures that the optimized droop control parameters can handle all possible scenarios resulting from the RES uncertainties. The proposed S-M-GBD enhances the convergence rate in solving the scenario-based OPF model.

REFERENCES

[1] Feng W, Tjernberg L B, Mannikoff A, et al. A new approach for benefit evaluation of multiterminal VSC–HVDC using a proposed mixed AC/DC optimal power flow[J]. *IEEE Trans. Power Del.*, 2013, 29(1): 432-443.

[2] Aziz S, Peng J, Wang H, et al. Admm-based distributed optimization of hybrid mtdc-ac grid for determining smooth operation point[J]. *IEEE Access*, 2019, 7: 74238-74247.

[3] Venzke A, Chatzivasileiadis S. Convex relaxations of probabilistic AC optimal power flow for interconnected AC and HVDC grids[J]. *IEEE Trans. Power Syst.*, 2019, 34(4): 2706-2718.

[4] Engelmann A, Jiang Y, Mühlpfordt T, et al. Toward distributed OPF using ALADIN[J]. *IEEE Trans. Power Syst.*, 2018, 34(1): 584-594.

[5] Zhai J, Dai X, Jiang Y, et al. Distributed optimal power flow for VSC-MTDC meshed AC/DC grids using ALADIN[J]. *IEEE Trans. Power Syst.*, 2022, 37(6): 4861-4873.

[6] Javed U, Mughees N, Jawad M, et al. A systematic review of key challenges in hybrid HVAC–HVDC grids[J]. *Energies*, 2021, 14(17): 5451.

[7] Gan L, Low S H. Optimal power flow in direct current networks[J]. *IEEE Trans. Power Syst.*, 2014, 29(6): 2892-2904.

[8] Kocuk B, Dey S S, Sun X A. Strong SOCP relaxations for the optimal power flow problem[J]. *Oper. Res.*, 2016, 64(6): 1177-1196.

[9] Yang Z, Zhong H, Xia Q, et al. Optimal power flow based on successive linear approximation of power flow equations[J]. *IET Gener. Transm. Dis.*, 2016, 10(14): 3654-3662.

[10] Z You F, Grossmann I E. Multicut Benders decomposition algorithm for process supply chain planning under uncertainty[J]. *Ann. Oper. Res.*, 2013, 210: 191-211.

[11] Jabr R A. Linear decision rules for control of reactive power by distributed photovoltaic generators[J]. *IEEE Trans. Power Syst.*, 2017, 33(2): 2165-2174.

[12] Hijazi H, Coffrin C, Hentenryck P V. Convex quadratic relaxations for mixed-integer nonlinear programs in power systems[J]. *Math. Program. Comput.*, 2017, 9: 321-367.

[13] Cao Y, Wang W, Li Y, et al. A virtual synchronous generator control strategy for VSC-MTDC systems[J]. *IEEE Trans. Energy Conver.*, 2017, 33(2): 750-761.

[14] Li H, Lekić A, Li S, et al. Distribution network reconfiguration considering the impacts of local renewable generation and external power grid[J]. *IEEE Trans. Ind. Appl.*, 2023, 59(6): 7771-7788.

[15] Y. Zhang, X. Ai, J. Fang, et al. Two-stage reactive power optimization for distribution network with distributed generation based on extreme scenarios[J]. *Trans. China Electrotech. Soc.*, 2018, 33(2): 380–389.